Experimental evidence of transient growth of energy before airfoil flutter

P. Hémon, E. de Langre

Département de Mécanique, LadHyX, Ecole Polytechnique – CNRS, F-91128 Palaiseau Cedex, France

P. Schmid

Department of Applied Mathematics, University of Washington, Seattle, USA

Corresponding author

Pascal Hémon

LadHyX, Hydrodynamics Laboratory, Ecole Polytechnique – CNRS, F-91128 Palaiseau cedex, France

Tel. +33 (0)1 69 33 36 79 – Fax +33 (0)1 69 33 30 30

Email *pascal.hemon@ladhyx.polytechnique.fr*

Abstract

This paper presents an experimental evidence of the transient growth of energy for the coupled-mode flutter of an airfoil. The phenomenon occurs even in linearly stable dynamical systems. Its application is rather new in the context of fluid-structure interactions where only theoretical and numerical studies of transient growth exist. The experimental setup allows a NACA 0015 airfoil to oscillate in rotational and vertical degrees of freedom when it is submitted to airflow. Measurements consist of time

histories of the two motions by means of laser displacement sensors. Structural parameters are first estimated without wind. The transient evolution of energy is measured and amplification is observed for given sets of initial conditions. Experiments agree well with the numerical simulations based on the unsteady airfoil theory.

Keywords

Transient growth, flutter instability

Nomenclature

A_i	aeroelastic coefficients for pitching moment (i=1,.., 4)
b, c	span and chord of the profile (m)
C_z'	derivative of lift coefficient
d	distance between gravity centre G and rotation axis O (m)
E	mechanical energy (J)
F_z	lift force (N)
f	frequency (Hz)
H_i	aeroelastic coefficients for lift force (i=1,.., 4)
J_O	inertia of the rotational motion around O (kg.m^2)
k	stiffness (N.m/rad) or (N/m)
M_O	pitching moment at rotation axis O (N.m)
m	mass involved in the vertical motion (kg)
U	wind velocity (m/s)
U_c	critical wind velocity (onset of flutter) (m/s)
z	vertical coordinate of gravity centre (m)

α	angle of rotation (rad)
η	reduced structural damping
λ	eigenvalue ($rad^2.s^{-2}$)
ρ	air density ($kg.m^{-3}$)
ω	angular frequency ($rad.s^{-1}$)

Subscripts

0	initial conditions
1 or 2	coupled motions
z	pure vertical motion
α	pure rotational motion

1. Introduction

In linear flutter studies, it is common to assume that the system amplitude behaves exponentially in time, decaying or growing depending on the wind velocity. The analysis then follows a normal modes approach where the long time behaviour is sought, especially the critical value of the velocity which characterizes the limit between stable and unstable behaviour.

In the field of hydrodynamic stability (Butler & Farrel 1992) it has been found in recent years that energy growth can transiently occur in the subcritical range of linear systems. This was mathematically formalized by Schmid & Henningson (2001) and references

therein. This mechanism leads to an initial amplification of the energy of the system that subsequently decreases due to stable conditions. This is called transient growth of energy. It is a consequence of the non-orthogonality of the modes involved in the dynamics of the system. These modes, because of non conservative forces, interact in such a way that the energy of the stable system is transiently amplified before it exponentially decays at the rate of the least stable mode.

Theoretical and numerical studies were recently performed on various fluid-structure systems and showed the possibility of transient growth in this kind of applications (Schmid & de Langre 2003, Hémon & Noger 2004). From an engineering point of view, this might explain the premature structural fatigue encountered in structures that are submitted to wind. Another important feature of transient growth is that if the growth is large enough, a non linear instability can be triggered by amplitude effect even when the system is linearly stable at small amplitude. This scenario could be seen as a by-pass mechanism leading to flutter instability before the linear critical velocity.

The objective of this paper is to present for the first time an experimental evidence of transient growth for the coupled-mode flutter of an airfoil. Starting from this standard application, it is reasonable to believe that transient growth may be present for other kind of elongated structures in cross flow susceptible to coupled mode flutter. Preliminary results of this study were presented at the 5^{th} colloquium on Bluff Body Aerodynamics and Applications, Ottawa, Canada, July 11-15, 2004.

The paper is organized as follow. First we describe the studied airfoil flutter and the standard corresponding model. The experimental setup and the results are then described and discussed in section 3 in regards to numerical simulations of the problem.

2. Classical airfoil flutter

2.1 Structural modelling

We recall in this section the main features of the coupled flutter of an airfoil which can simultaneously oscillate transversely to the flow and in torsion, as presented Fig. 1. The rotation axis and the gravity centre are separated by the distance d which induces structural coupling between the two degrees of freedom z and α. The motion equations read (see Fung, 1993)

$$\begin{aligned} & m\,\ddot{z} + 2m\eta_z\omega_z\,\dot{z} + k_z\,z + m\,d\,\ddot{\alpha} = F_z \\ & J_O\,\ddot{\alpha} + 2\,J_O\,\eta_\alpha\,\omega_\alpha\,\dot{\alpha} + k_\alpha\,\alpha + m\,d\,\ddot{z} = M_O \end{aligned}, \tag{1}$$

The eigenvalues for the non-coupled case (d=0) are

$$\begin{aligned} \lambda_\alpha &= \omega_\alpha{}^2 = (2\pi\,f_\alpha)^2 = k_\alpha / J_O \\ \lambda_z &= \omega_z{}^2 = (2\pi\,f_z)^2 = k_z / m \end{aligned}. \tag{2}$$

In the more general coupled case can be shown that the distance d between the gravity centre and the rotation axis modifies the eigenvalues so that

$$\lambda_1 + \lambda_2 = \lambda_z + \lambda_\alpha \frac{1}{1 - md^2/J_O}, \tag{3}$$

where the eigenvalues of the coupled system are λ_1 and λ_2.

The total energy is the sum of kinetic and potential energy which reads:

$$E(t) = \frac{1}{2} m\,\dot{z}^2(t) + \frac{1}{2} J_O\,\dot{\alpha}^2(t) + m\,d\,\dot{\alpha}(t)\,\dot{z}(t) + \frac{1}{2} k_z\,z^2(t) + \frac{1}{2} k_\alpha\,\alpha^2(t). \tag{4}$$

This quantity will be used to quantify the transient growth. It will be made dimensionless by reference to the initial energy E_0 estimated with the applied initial conditions. The maximum value of $E(t)$ observed along the time histories will be noted E_{max}.

2.2 Aerodynamic effect

The linear aerodynamic loads can be modelized using Scanlan's flutter derivatives (1977)

$$\begin{aligned} F_z &= \frac{1}{2}\rho b c U^2 \left(H_1\, \dot{z} + H_2\, \dot{\alpha} + H_3\, \alpha + H_4\, z\right) \\ M_O &= \frac{1}{2}\rho b c^2\, U^2 \left(A_1\, \dot{z} + A_2\, \dot{\alpha} + A_3\, \alpha + A_4\, z\right) \end{aligned}, \tag{5}$$

where the flutter derivatives can be expressed with the help of the Unsteady Airfoil Theory (UAT). The reduced velocity is defined by reference with the profile chord and the frequency of each pure motion, *i.e.*

$$U_r = U \big/ c\, f_z \quad \text{or} \quad U_r = U \big/ c\, f_\alpha \,. \tag{6}$$

All the coefficients of equation (5) are expressed using the Theodorsen function (Theodorsen, 1935) $C(K) = F(K) + iG(K)$ where the reduced circular frequency is $K = 2\pi / U_r$. After rearrangement this leads to (Fung, 1993)

$$\begin{aligned} H_1 &= \frac{-1}{U} C_z{}' \, F; \qquad H_2 = \frac{c}{U} C_z{}' \left[\frac{1}{4} + \frac{G}{K} + \frac{F}{2}\left(\frac{1}{2} - a\right)\right]; \\ H_3 &= C_z{}' \left[F - \frac{KG}{2}\left(\frac{1}{2} - a\right) + K^2 \frac{a}{8}\right]; \qquad H_4 = \frac{1}{c} C_z{}' \left[\frac{1}{4} + \frac{G}{K}\right] K^2 \\ A_1 &= \frac{-1}{U} C_z{}' \, \frac{F}{2}\left(\frac{1}{2} + a\right); \qquad A_2 = \frac{c}{U} C_z{}' \left[\frac{1}{8}\left(\frac{1}{2} - a\right) - \frac{G}{K}\frac{1}{2}\left(\frac{1}{2} + a\right) + \frac{F}{4}\left(a^2 - \frac{1}{4}\right)\right] \\ A_3 &= C_z{}' \left[\frac{1}{16}\left(a^2 + \frac{1}{8}\right) K^2 + \frac{F}{2}\left(\frac{1}{2} + a\right) + \frac{KG}{4}\left(a^2 - \frac{1}{4}\right)\right]; \quad A_4 = C_z{}' \frac{K^2}{2c}\left[\frac{a}{4} + \frac{G}{K}\left(\frac{1}{2} + a\right)\right] \end{aligned} \,. \tag{7}$$

The parameter *a* is the dimensionless distance between the rotation axis O and the mid-chord location based on a reference length *c*/2. It is therefore equal to -1/2 in our case. Note also that for a NACA 0015 profile, the aerodynamic centre is located at the forward quarter-chord point, which is also the rotation axis O.

In practice, the terms H_4 and A_4 are of negligible influence for our study range at large reduced velocities. Moreover, it can be useful to introduce the Quasi-Steady Theory assumption (QST) in order to simplify the above expressions, hence

$$\begin{aligned} &H_1 = \frac{-1}{U} C_z' ; \quad H_2 = 0 ; \qquad H_3 = C_z' ; \quad H_4 = 0 \\ &A_1 = 0 ; \qquad A_2 = \frac{-1}{8} \frac{c}{U} C_z' ; \quad A_3 = 0 ; \qquad A_4 = 0 \end{aligned} . \tag{8}$$

The static lift derivative C_z' is theoretically equal to 2π for a thin profile at low angle of attack within the assumptions of potential flow. But in practice its value depends on the Reynolds number, especially in the low range of our experiments.

Combining (1), (5) and (8) we have

$$\begin{aligned} &\ddot{z} + 2\omega_z \left(\eta_z + \eta_{a_z}\right) \dot{z} + \omega_z^{\,2}\, z + d\, \ddot{\alpha} = \frac{\rho b\, U_r^{\,2}}{2 c f_z^{\,2} m} C_z'\, \alpha \\ &\ddot{\alpha} + 2\omega_\alpha \left(\eta_\alpha + \eta_{a\alpha}\right) \dot{\alpha} + \omega_\alpha^{\,2} \alpha + \frac{m d}{J_O}\, \ddot{z} = 0 \end{aligned} \tag{9}$$

in which the pure added aerodynamic damping have been rewritten in the form of reduced damping, such that

$$\eta_{a_z} = \frac{\rho b c^2}{2m} U_r ; \quad \eta_{a\alpha} = \frac{\rho b c^4}{64 J_O} U_r . \tag{10}$$

2.3 Critical flutter velocity of the undamped system

In a first step, the critical velocity is deduced from the undamped coupled system (9) which is reduced to

$$\begin{aligned} &\ddot{z} + \omega_z^{\,2}\, z + d\, \ddot{\alpha} = \frac{\rho b\, U_r^{\,2}}{2 c f_z^{\,2} m} C_z'\, \alpha \\ &\ddot{\alpha} + \omega_\alpha^{\,2} \alpha + \frac{m d}{J_O}\, \ddot{z} = 0 \end{aligned} . \tag{11}$$

The onset of flutter for this system arises when the eigenvalues become complex, the two frequencies becoming equal. It occurs when

$$\det\begin{vmatrix} \lambda-\lambda_z & \lambda d+\dfrac{\rho b {U_r}^2}{2c{f_z}^2 m}H_3 \\ \dfrac{\lambda m d}{J_O} & \lambda-\lambda_\alpha \end{vmatrix}=0\,. \tag{12}$$

This leads to finding the smallest root U^2 of the second order equation

$$\left(\lambda_z+\lambda_\alpha+\frac{d\ \rho\ bc\,U^2}{2\ J_O}C_z{}'\right)^2-4\,\lambda_\alpha\,\lambda_z\left(1-\frac{md^2}{J_O}\right)=0\,. \tag{13}$$

The critical velocity is finally given by

$${U_c}^2=\frac{-2\,J_O\left(-(\lambda_z+\lambda_\alpha)+\sqrt{4\,\lambda_\alpha\,\lambda_z\,\dfrac{\lambda_z+\lambda_\alpha}{\lambda_1+\lambda_2}}\right)}{\rho\ b\ c\ d\ C_z{}'}, \tag{14}$$

and the frequency of flutter, determined for the critical velocity, reads

$${f_c}^2=\frac{1}{(2\pi)^2}\sqrt{\lambda_\alpha\,\lambda_z\,\frac{\lambda_1+\lambda_2}{\lambda_z+\lambda_\alpha}}\,. \tag{15}$$

3. Experimental evidence

3.1 Experimental setup

The wing profile is a NACA 0015 with a chord 0.12 m and 0.17 m span. It is built with plexiglas by means of a numerical milling machine. The resulting surface is smooth as a mirror without artificial roughness. The profile is mounted in a small Eiffel wind tunnel of closed square test section of 0.180 m width. Wind stream is produced by a centrifugal fan of electric power 2500 W mounted downstream and exhausting the air flow

vertically. Mean velocity in the test section can vary from 2 to 25 m/s, with a turbulence level of 1.5 % at 10 m/s.

The rotation axis of the profile is located at its forward quarter-chord and pass through the wind tunnel walls within two vertical fences. The axis is suspended via bearings at the extremities of two long flat sticks of aluminium alloy, such as laminated springs (see Fig. 2). Their length is 400 mm, 20 mm width and 2 mm thickness. Adjustment of the frequency was done by adjusting the thickness to around 1 mm near the clamping using a milling machine. The torsion frequency is set by two series of linear springs.

The measurements are based on two laser displacement sensors, one for the vertical bending motion, and the other one for the combined movement of torsion and bending. Resolution is 40 μm and accuracy better than 1% of their full scale range (±10 mm). The output signals of these sensors are digitized with a PAK system provided by Müller BBM (24 bits resolution). The sampling frequency was chosen to be 512 Hz and a DC coupling is used in both channels. Recombination of the physical quantities in terms of vertical position, angle of torsion and energy is performed directly in the measurement system by numerical post-processing.

Transient records are triggered automatically so that the starting point is repeatable, and initial conditions are recorded through the DC coupling of the measurement chain. Note that in the computation of the energy it is essential to ensure that the system at rest (without wind) provides a zero constant signal, due to the necessary derivation process for obtaining the velocities.

3.2 Identification of structural parameters

The structural parameters are identified without wind. First we deal with the two motions separately. We measure the natural frequencies f_α, f_z by spectral analysis and stiffness k_α, k_z by static calibration. Then we deduce the inertia J_O, m from equation (2).

The frequencies f_1, f_2 of the coupled system are then measured and the distance d is deduced from equation (3). All the results are given in Table 1.

Structural damping is measured for each degree of freedom independently. For vertical motion, the system is mechanically very pure with a low damping, η_z = 0.40 %. For torsion, the mechanical assembly, especially the bearings, provides damping which is found to be a function of the amplitude of the oscillations. It varies from 10 % for amplitude around 2° to 6 % for higher amplitudes around 7°.

In order to validate all these results, we reproduce by numerical simulation an experimental test without wind and we compare the results in Fig. 3. The initial condition is a small vertical offset downward, leading to a non-zero initial value for z and small positive angle of torsion, as a consequence of the coupled mechanical system. It must be mentioned here that because of the laminated spring, a vertical displacement induces a small angle of rotation, which is taken into account in the recombination procedure of the pitch angle α.

In the experiments, the dimensionless energy referred to the initial conditions is weakly perturbed by the DC value of the measured components, leading to a non perfectly monotonic decay. It will be seen later that these perturbations can be considered as a noise and that the signal to observe is much larger. In Fig. 3, the comparison between experimental and numerical results is very good and thus validates the measured structural parameters values.

3.3 Identification of aerodynamic damping and critical velocity

The experimental critical velocity U_c, determined is found to be 9.0 m/s, in comparison with 7.83 m/s given by equation (14) using the lift slope $C_z' = 2\pi$. Two reasons may cause the difference: (i) the effect of damping, especially in torsion, which has a stabilizing effect and increases the critical velocity; (ii) a Reynolds number effect (Re = 72000 at the onset of flutter) because the boundary layer laminar - turbulent transition on the profile has a significant influence on the lift slope at this regime.

However, the numerical simulations of the full modelling (7) leads to a critical velocity equal to 9.28 m/s in very good agreement with the experiments. Therefore the numerical simulations shown later in this paper will be based on equation (7), taking into account all the terms.

Good agreement is obtained in terms of flutter frequency: 3.26 Hz (experimental), versus 3.145 Hz (equation 15). Note that this frequency was experimentally determined at a velocity just before the onset of flutter, in order to make the measurements with a non diverging system.

For the added damping, agreement with the relations (10) and experiments is also good. For vertical motion, the experimental value is 1.98 % at U_r=21, against 1.82 % theoretically. In torsion, the added damping at U_r=29 is around 3.5 % against 4.52 % theoretically, but with a high experimental uncertainty due to the high structural damping at zero velocity.

3.4 Transient growth measurements

We apply now the initial conditions in z and α as described above on the system with several wind velocities just under the critical velocity. A typical time history is shown Fig. 4 where it appears clearly an amplification of the energy of a factor of about 2. Simultaneously, the angle of attack reaches a value of almost 6° while it was remaining under 4° without wind, see Fig. 3. This is consistent with the fact that an amplification of energy of a factor 2 induces an amplification of a factor $\sqrt{2}$ of the displacement

The maximum amplification of the energy is plotted in Fig. 5 for a number of tests versus the velocity parameter $1 - U/U_c$ as defined by Schmid & de Langre (2003). In the experiments, the amplification occurs for velocity parameters below 0.30 and the amplification reaches a saturation value of about 2.5 just before flutter.

The numerical simulation using the UAT (equation 7) provides here a remarkable agreement with the experiments. This shows that for the transient behavior simulation, it is essential to account for all the coefficients H_i and A_i, including those that are usually considered negligible in the long term stability problem.

3.5 Effect of the initial conditions

We now use a different set of initial conditions. The experimental procedure consists in letting a small mass (50 g) falling on the profile from a given height. The measurement trigger remains performed automatically with one of the channels. The purpose is to introduce initial conditions in $\dot{\alpha}$ and $\dot{z}$ with the best possible repeatability.

Finally this technique leads to a set of initial conditions $z_0 = 0.5$ mm, $\alpha_0 = -1.6°$, $\dot{z}_0 = -38$ mm/s and $\dot{\alpha}_0 = -60$ °/s. The maximum amplification of the energy is plotted Fig. 6

versus the velocity parameter. The amplification is roughly half of that obtained with the previous initial conditions. The measurements are much more difficult to perform with repeatability because now the profile is free to vibrate with the upstream turbulence before the trigger, whereas it was fixed in the previous case. This explains the lack of experimental data near the onset of flutter, because it was not possible to correctly perform the initial conditions without large uncertainty. However the numerical simulations provide once again a satisfactory comparison with the experiments.

It has been found interesting to search numerically the set of initial conditions that would lead to the maximum amplification rate. These optimal initial conditions were found to be z_0 = -2 mm, α_0 = 6°, $\dot{z}_0$ = 0 mm/s and $\dot{\alpha}_0$ = 0 °/s. The corresponding amplification is shown in Fig. 7. We observe a saturation value of 4.6 which is quite a large amplification. It is shown that the transient growth can really induce higher stresses in the structure than it is usually admitted for a stable aeroelastic system. From an engineering point of view, a study of transient growth of energy should be included in the design process of a structure, especially for the fatigue effects. It is also possible that a by-pass transition to an instable regime can occur for systems having a subcritical instable nonlinear branch.

4. Summary

We have presented an experimental evidence of transient growth of energy before coupled-mode flutter of an airfoil. This mechanism was shown to exist before in various fluid-structure systems using theoretical and numerical simulation but without

experimental proof. An experimental setup was presented which allows a NACA 0015 profile to oscillate in vertical motion and in torsion. The transient behaviour of this system following given initial conditions showed a transient amplification of energy before the usual exponential decay. The unsteady airfoil theory was found capable to reliably capture the phenomenon when all the terms are included in the simulations. This phenomenon might explain some premature fatigue of wind excited structures. Moreover, it could be responsible of a by-pass transition to instable regime by nonlinear amplitude effect. A study of this type is therefore recommended for the fatigue analysis of structures that are submitted to wind loads.

References

Butler, K. M., Farrel, B. F. 1992. Three dimensional optimal perturbation in viscous shear flow. Physics of Fluids A, 4, 1637-1650.

Fung, Y.C. 1993 An introduction to the theory of aeroelasticity. Dover, New York.

Hémon, P., Noger, C. 2004. Transient growth of energy and aeroelastic stability of ground vehicles. *Comptes Rendus Mécanique* 332, 175-180.

Scanlan, R. H., Tomko, J. J. 1977 Airfoil and bridge deck flutter derivatives. *ASCE Journal of the Engineering Mechanics Division*, December, 1717-1737.

Schmid, P. J., de Langre E. 2003 Transient growth before coupled-mode flutter. *ASME Journal of Applied Mechanics* 70, 894-901.

Schmid, P. J., Henningson, D. S. 2001. Stability and transition in shear flows. Springer, New York.

Theodorsen, T. 1935 General theory of aerodynamic instability and the mechanism of flutter. NACA Technical Report 496.

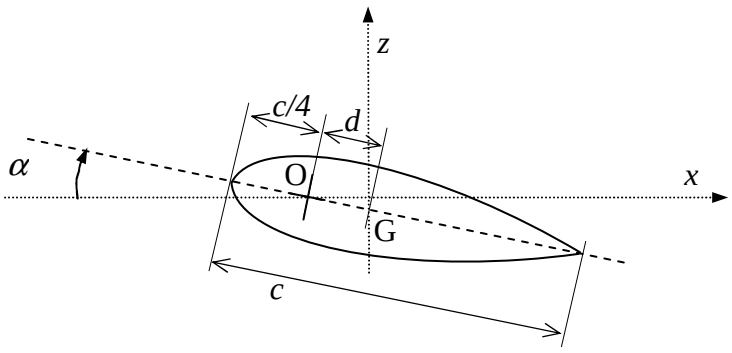

Fig. 1. Airfoil geometry

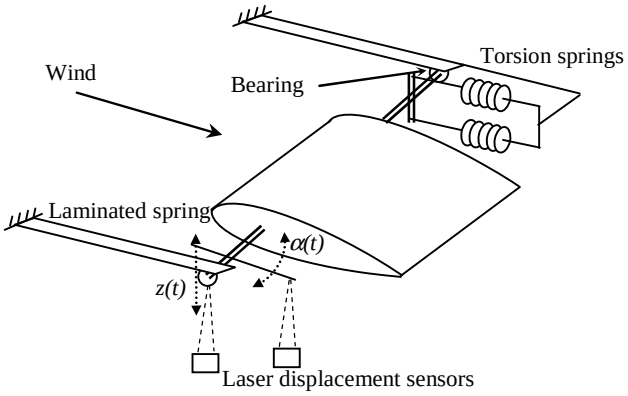

Fig. 2. Experimental setup

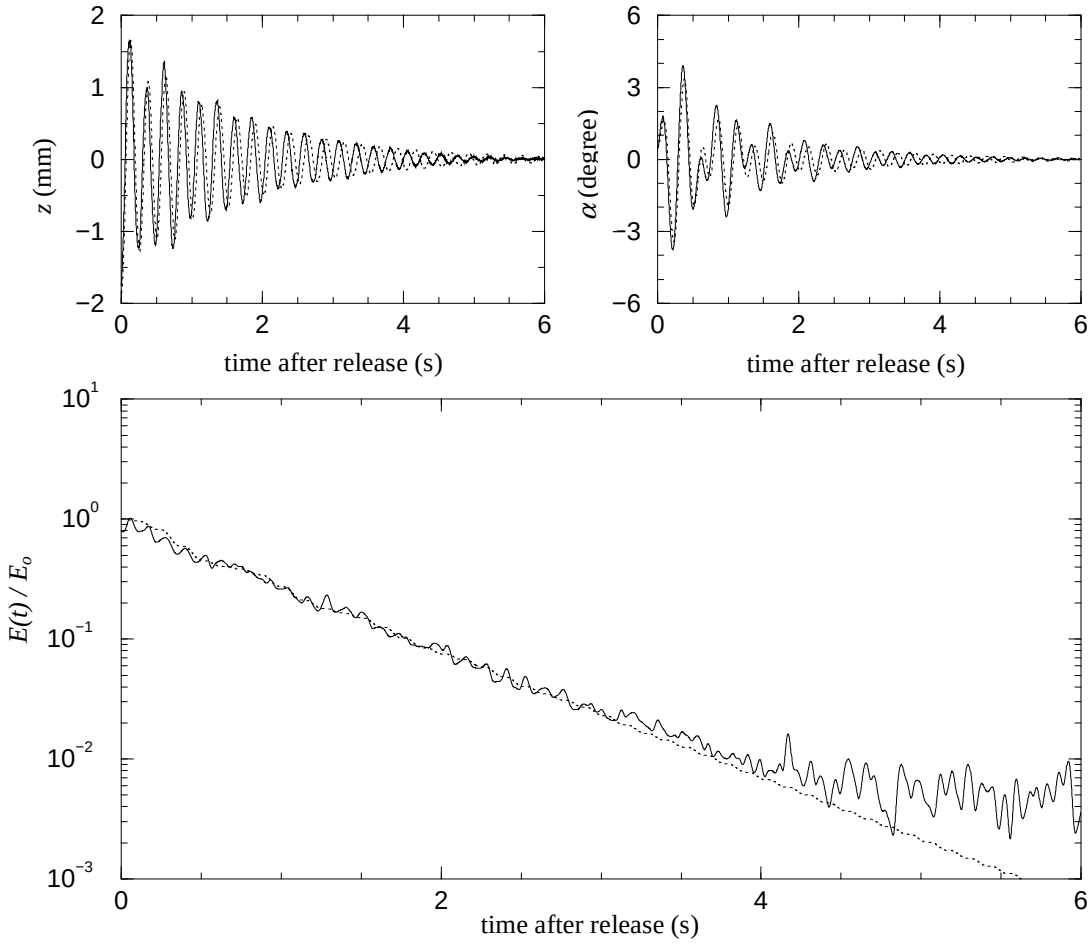

Fig. 3. Time history of vertical displacement, angle of rotation and corresponding dimensionless total energy without wind (U=0). Initial conditions are z_0 = -1.85 mm, α_0 = 0.5°. (——) experiments; (.....) computation using equation (1).

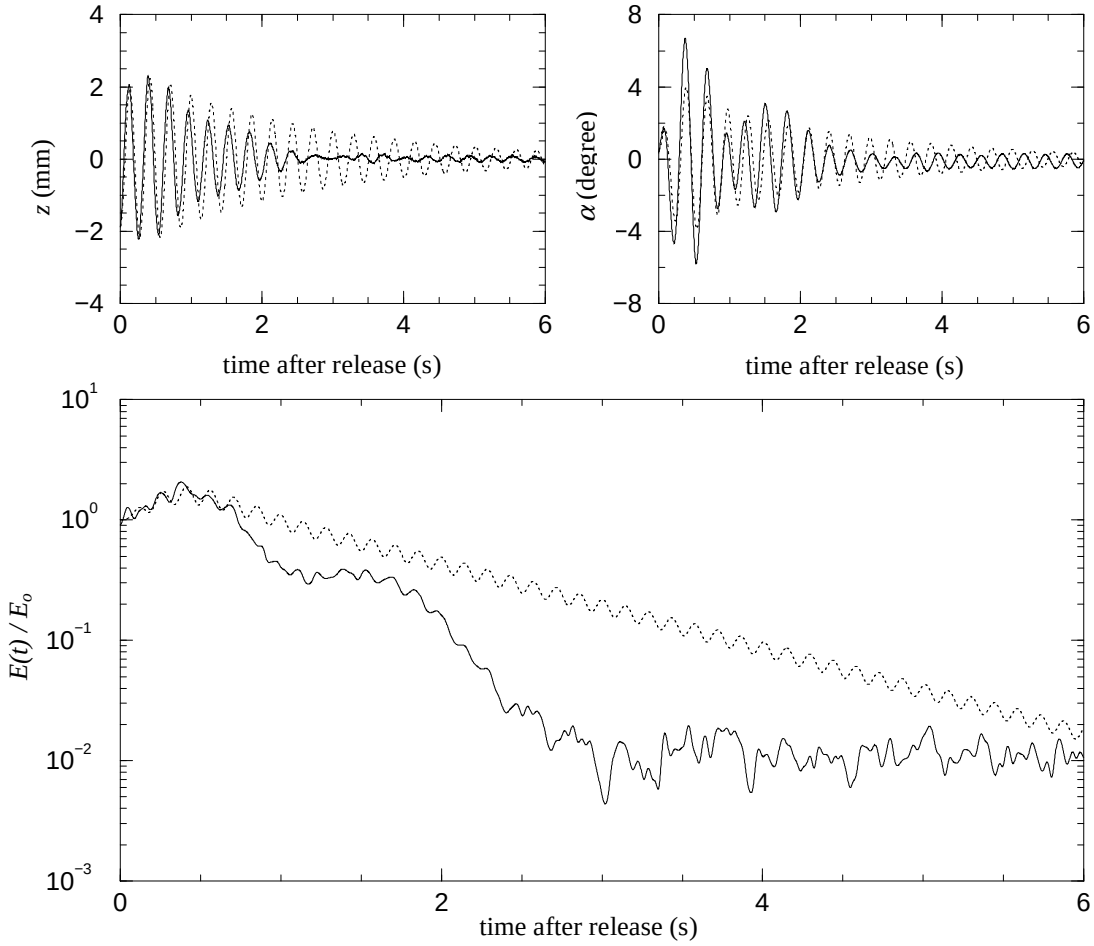

Fig. 4. Time history of vertical displacement, angle of rotation and corresponding dimensionless total energy with U/U_c = 0.92. Initial conditions as in Fig 3. (___) experiments; (.....) computation using UAT, equations (1), (5) and (7).

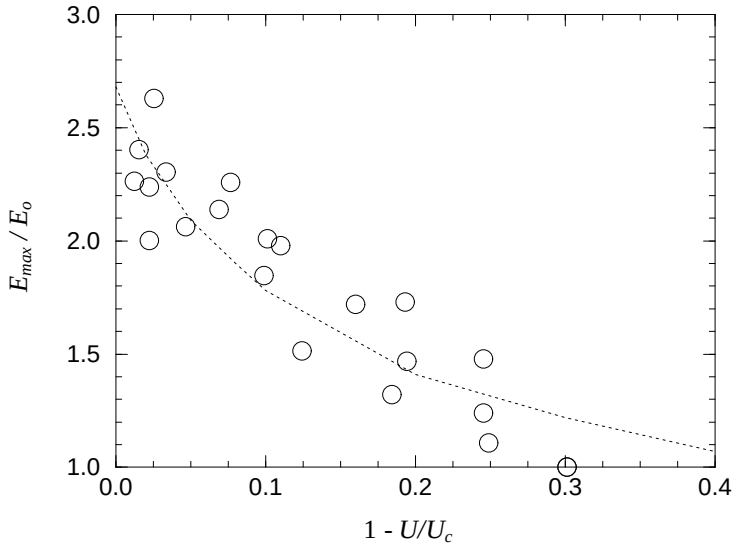

Fig. 5. Maximum amplification of energy E_{max} / E_0 versus velocity parameter 1 – U/U_c for initial conditions z_0 = -1.85 mm and α_0 = 0.5°. (○) experiments; (.....) computations using UAT.

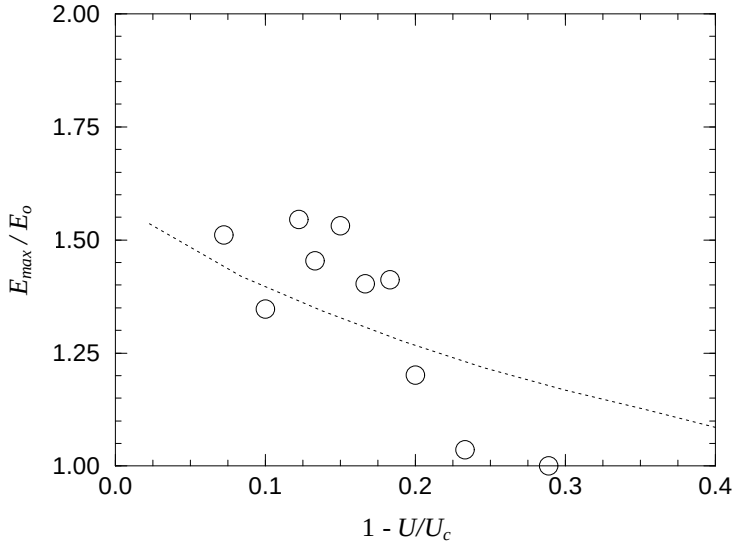

Fig. 6. Maximum amplification of energy E_{max} / E_0 versus velocity parameter 1 – U/U_c for initial conditions z_0 = 0.5 mm, α_0 = -1.6°, $\dot{z}_0$ = -38 mm/s and $\dot{\alpha}_0$ = -60 °/s. (○) experiments; (.....) computations using UAT.

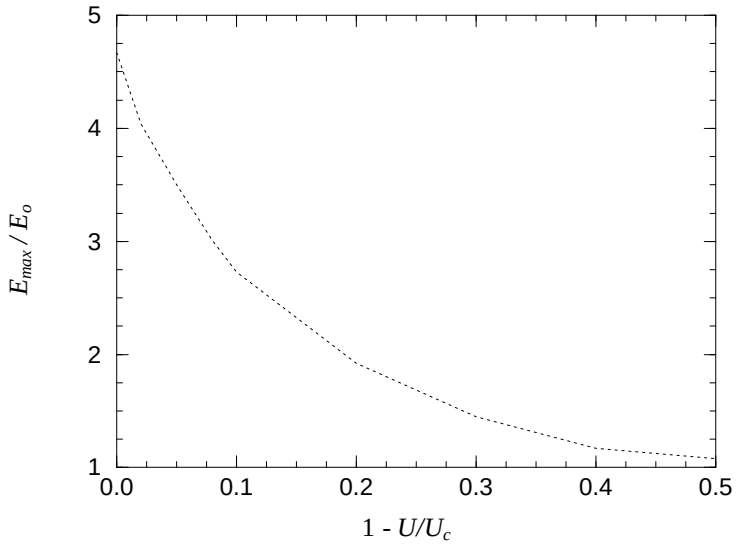

Fig. 7. Maximum amplification of energy E_{max} / E_0 versus velocity parameter $1 - U/U_c$. Computations using UAT for optimal initial conditions z_0 = -2 mm and α_0 = + 6°.

Table 1. Measured structural parameters

f_α (Hz)	f_z (Hz)	k_α (N.m/rad)	k_z (N/m)	f_1 (Hz)	f_2 (Hz)	J_O (kg.m^2)	m (kg)	d (m)
2.597	3.613	0.1140	436.0	2.441	4.004	0.00042365	0.846	-0.00706